J|A|C|S
ARTICLES
Published on Web 10/21/2006

Atoms-in-Molecules Study of Intra- and Intermolecular Bonding in the Pentaerythritol Tetranitrate Crystal

Elizabeth A. Zhurova,[†] Adam I. Stash,[†,‡] Vladimir G. Tsirelson,[§] Vladimir V. Zhurov,[†] Ekaterina V. Bartashevich,[||] Vladimir A. Potemkin,[||] and A. Alan Pinkerton*[,†]

Contribution from the Department of Chemistry, University of Toledo, Toledo, Ohio 43606, Karpov Institute of Physical Chemistry, Moscow, Russia, Mendeleev University of Chemical Technology, Moscow, Russia, and Chelyabinsk State University, Chelyabinsk, Russia

Received August 19, 2006; E-mail: apinker@uoft02.utoledo.edu

Abstract: Chemical bonding in the pentaerythritol tetranitrate crystal based on the experimental electron density obtained from X-ray diffraction data at 100 K and theoretical calculations at the experimental molecular geometry have been analyzed in terms of the Quantum Theory of Atoms in Molecules. Features of the intra- and intermolecular bond critical points and the oxygen atom lone-pair locations are discussed. Numerous intermolecular bonding interactions, including O···H and O···O, have been found and characterized. Atomic charges and atomic energies were integrated and compared with those for similar compounds. The N−O topological bond orders have been calculated for the first time, and the PETN atomic valences have been estimated.

Introduction

Because of the growing interest in the development of new energetic materials (explosives, propellants), there is a need to understand their behavior based on their microscopic properties.[1−3] In the past few years, we have undertaken a program to relate the properties of energetic crystals with their structure and their electron-density distribution features.[2,4−9] One of the energetic materials, pentaerythritol tetranitrate (PETN), is of particular interest from this point of view. It is extensively used as "an initiating or booster high explosive".[10] PETN is a relatively sensitive explosive (h_{50} = 12 cm),[11,12] but is stable enough to perform X-ray diffraction experiments with caution. It exists in two polymorphs[13] with a phase transition (PETN−I to PETN−II) temperature ∼410 K. In this paper, we present the results from a low-temperature X-ray diffraction experiment, as well as from a solid state theoretical calculation of PETN. Our analysis of the chemical bonding in the PETN crystal exploits the terms and notions of the Quantum Theory of Atoms in Molecules (QTAIM).[14] The deformation electron density maps are also discussed.

Experimental Measurements and Data Refinements.

Data Collection and Reduction. A colorless PETN−I crystal specimen was mounted on a 0.1 mm capillary and cooled to 100 K with an Oxford Cryostream cooling device. The X-ray diffraction experiment was performed using a Bruker platform diffractometer with Mo radiation and a SMART 6000 CCD detector. ω−scans with a 0.3° step were performed at a detector distance ∼3.22 cm. A detector setting of $2\theta = -53°$ and several different φ settings were used. Because of severe "bleeding" of the strongest reflections, the data have been measured twice with 15 and 60 s exposure times. Then, "bleeding" reflections were removed from the 60 s data subset (integrated with a pixel mask $2\theta = 0-14°$), and the two subsets were scaled together. The first 100 frames were repeated at the end of measurement, and no X-ray intensity decay was found. Data integration and unit cell refinement were performed with the program *SAINT*.[15] An empirically chosen integration box size of 1.5 × 1.5 × 0.75° and a profile fitting procedure based on strong ($I > 20\sigma$) reflections allowed us to obtain the best internal consistency (R_{int} = 0.0202). The data were corrected for oblique incidence[16] and averaged (scaled and merged) with the program *SORTAV*.[17,18] Other experimental details are presented in Table 1.

[†] University of Toledo.
[‡] Karpov Institute of Physical Chemistry.
[§] Mendeleev University of Chemical Technology.
[||] Chelyabinsk State University.

(1) Politzer, P., Murray, J. S., Eds. *Energetic Materials*; Theoretical and Computational Chemistry Series, Vol. 12; Elsevier: New York, 2003.
(2) Pinkerton, A. A.; Ritchie, J. P. *J. Mol. Struct.* **2003**, *657*, 57−74.
(3) Tanbug, R.; Kirschbaum, K.; Pinkerton, A. A. *J. Chem. Cryst.* **1999**, *29*, 45−55.
(4) Zhurova, E. A.; Pinkerton, A. A. *Acta Crystallogr.* **2001**, *B57*, 359−365.
(5) Zhurova, E. A.; Martin, A.; Pinkerton, A. A. *J. Am. Chem. Soc.* **2002**, *124*, 8741−8750.
(6) Zhurova, E. A.; Tsirelson, V. G.; Stash, A. I.; Pinkerton, A. A. *J. Am. Chem. Soc.* **2002**, *124*, 4574−4575.
(7) Ritchie, J. P.; Zhurova, E. A.; Martin, A.; Pinkerton, A. A. *J. Phys. Chem.* **2003**, *B107*, 14576−14589.
(8) Zhurova, E. A.; Tsirelson, V. G.; Stash, A. I.; Yakovlev, M. V.; Pinkerton, A. A. *J. Phys. Chem.* **2004**, *B108*, 20173−20179.
(9) Chen, Y.-S.; Stash, A. I.; Pinkerton, A. A., submitted for publication, **2006**.
(10) Gruzdkov, Yu. A.; Gupta, Y. M. *J. Phys. Chem. A* **2000**, *104*, 11169−11176.
(11) Storm, C. B.; Stine, J. R.; Kramer, J. F. *Chemistry and Physics of Energetic Materials*; Bulusu, S. N., Ed.; Kluwer Academic Publishers: Norwell, MA, 1990; pp 605−639.
(12) The shorter the impact drop height, h_{50}, the greater is the sensitivity. For example, quite sensitive RDX and HMX have h_{50} of 24 and 26 cm respectively, and the less sensitive NTO has h_{50} = 291 cm (ref 11).
(13) Cady, H. H.; Larson, A. C. *Acta Crystallogr.* **1975**, *B31*, 1864−1869.
(14) Bader, R. F. W. *Atoms in Molecules: A Quantum Theory*; The International Series of Monographs of Chemistry; Halpen, J., Green, M. L. H., Eds.; Oxford: Clarendon Press: Oxford, 1990; pp 1−438.
(15) Siemens, *SAINT*. Program to Integrate and Reduce Raw Crystallographic Area Detector Data 1996.
(16) Zaleski, J.; Wu, G.; Coppens, P. *J. Appl. Crystallogr.* **1998**, *31*, 302−304.

10.1021/ja0658620 CCC: $33.50

Table 1. Experimental Details

empirical formula	$C_5H_8O_{12}N_4$
temperature (K)	100.0(1)
crystal size (mm)	0.22 × 0.25 × 0.30
crystal shape	prism
wavelength (Å)	0.71073
crystal system	tetragonal
space group	$P\bar{4}2_1c$
unit cell dimensions (Å)	$a = 9.2759(8)$, $c = 6.6127(4)$
V (Å^3), Z	568.97, 2
D_{calc} (g cm^{-3})	1.845
μ (mm^{-1})	0.19
$(\sin\theta/\lambda)_{max}$ (Å^{-1})	1.098
reflections integrated	103588
R_{int}/average data multiplicity	0.0202/30.7
independent reflections	3339
overall completeness, %	100
independent reflections used ($\|F\|>3\sigma$)	3226
refinement based on	F
total number of parameters	205
final $R(F)$ indices:	
spherical atom refinement ($\|F\|>4\sigma$)	0.0255
aspherical atom refinement ($\|F\|>3\sigma$)	0.0104
goodness_of_fit	1.168

Refinements. The PETN−I crystal structure has been reported before.[13,19−21] From our experimental data at 100 K, the crystal structure was resolved by direct methods, and a preliminary least-squares refinement was carried out with the *SHELXTL* program suite.[22] The positions of hydrogen atoms at this stage were determined from the difference Fourier peaks. Anisotropic thermal motion was considered for all non-hydrogen atoms, and the latter were refined isotropically. Then, a multipole model[23] refinement using the *MOLDOS2004*[24] and *XD*[25] program packages was performed. For the O and C atoms, the multipole refinement was performed up to the hexadecapole level and for H atoms, up to the quadrupole level. The molecule electroneutrality condition was imposed throughout the refinement. For the hydrogen atoms, the fixed expansion/contraction parameters $\kappa = \kappa' = 1.2$ were chosen. The C−H bond lengths were fixed to the tabulated value of 1.09 Å.[26] Highly correlated parameters were refined in separate groups; the refinement procedure was stable, and full convergence of all parameters has been reached.

Evaluation of Data Quality. From the experimental data, the rigid-bond test[27] showed that the differences of mean-square displacement amplitudes along the interatomic vectors were less than 1.5×10^{-4} Å^2. The ratios of observed and calculated structure factors averaged over separate regions of reciprocal space were very close to unity (within 1%),[28] indicating a correct scale factor for all data as well as good model fitting for the whole sin θ/λ range. The residual electron density (the Fourier difference between observed and calculated multipole electron densities: $\delta\rho_{resid} = \rho_{exper} - \rho_{mult}$) showed no peaks above or below 0.049/−0.093 eÅ^{-3}. The total electron density was non-negative everywhere in space.

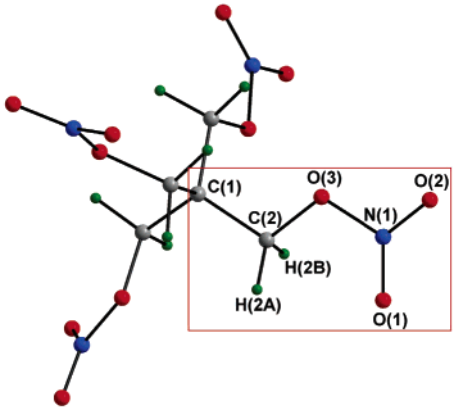

Figure 1. PETN molecule.

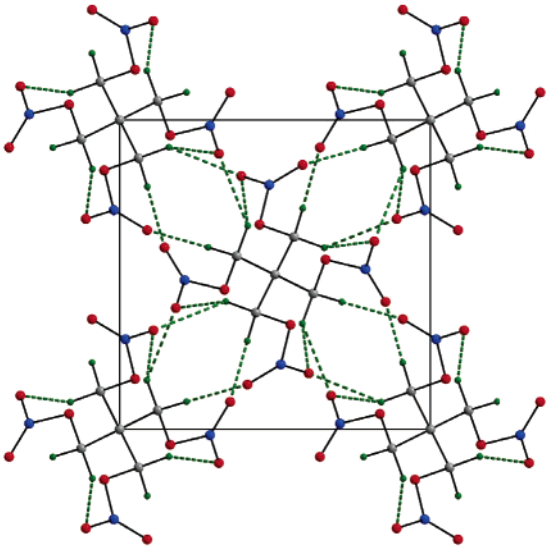

Figure 2. PETN packing diagram showing hydrogen bonds as green dashed lines − projection down the *c*-axis. Atoms are colored as shown in Figure 1.

The PETN molecule is shown in Figure 1, and a view of crystal packing and hydrogen bond pattern is presented in Figure 2. The total electron density and derived properties have been analyzed using the program package *WinXPRO*[29,30]

Theoretical Calculations

The DFT/B3LYP/6-311G(d,p) periodic theoretical calculation was performed with the program *CRYSTAL98*[31] at a molecular geometry fixed at that observed experimentally. Theoretical structure factors have been calculated for all possible *hkl* indices up to sin $\theta/\lambda = 1.0$ Å^{-1} and used for a multipole-model refinement in the same manner[32] as the experimental data. The final $R(F) = 0.0036$ was reached. The residual electron density showed no peaks above or below 0.063/−0.060 eÅ^{-3}.

(17) Blessing, R. H. *Cryst. Rev.* **1987**, *1*, 3−58.
(18) Blessing, R. H. *J. Appl. Crystallogr.* **1989**, *22*, 396−397.
(19) Booth, A. D.; Llewellyn, F. J. *J. Chem. Soc.* **1947**, 837−846.
(20) Trotter, J. *Acta Crystallogr.* **1963**, *16*, 698−699.
(21) Nieger, M.; Lehmann, J. *Cambridge Structural Data Base* (entry PERYTN11 **2002**).
(22) Sheldrick, G. M. *SHELXTL*, Vers. 6.14: An Integrated System for Solving, Refining and Displaying Crystal Structures from Diffraction Data; University of Göttingen: Germany, 2000.
(23) Hansen, N.; Coppens, P. *Acta Crystallogr.* **1978**, *A34*, 909−921.
(24) Stash, A. I. *Proc. for the 28th ISTC Japan Workshop on Frotiers of X-ray Diffraction Technologies*, Russia/CI,: Nagoya, 2003; pp 147153, modified version of the programs *MOLLY* (ref 22) and *MOLDOS97/MOLLY PC-DOS*, version 01; Protas, J., Ed.; University Henri-Poincare-Nancy I: Nancy, 1997.
(25) Koritsanszky, T.; Richter, T.; Macchi, P.; Gatti, C.; Howard, S.; Mallinson, P. R.; Farrugia, L.; Su, Z. W.; Hansen, N. K. *XD − A Computer Program Package for Multipole Refinement and Analysis of Electron Densities from Diffraction Data*; Technol. Rep.; Freie Universität Berlin: Berlin, Germany, 2003.
(26) Allen, F. H.; Kennard, O.; Watson, D. G.; Brammer, L.; Orpen, A. G.; Taylor, R. *J. Chem. Soc., Perkin Trans.* **1987**, *2*, S1−S19.
(27) Hirshfeld, F. L. *Acta Crystallogr.* **1976**, *A32*, 239−244.
(28) Experimental intensity of the strongest (201) reflection was underestimated by 4.4% due to a very light "bleeding" even at 15′ exposure time.
(29) Stash, A. I.; Tsirelson, V. G. *J. Appl. Crystallogr.* **2002**, *35*, 371−373.
(30) Stash, A. I.; Tsirelson, V. G. *Crystallogr. Reports* **2005**, *50*, 202−209.
(31) Saunders: V. R.; Dovesi, R.; Roetti, C.; Causà, M.; Harrison, N. M.; Orlando, R.; Sicovich-Wilson, C. M. *CRYSTAL98 User's Manual*; University of Torino: Torino, 1998.
(32) Only multipole model parameters have been refined for the theoretical data.

Table 2. PETN Geometrical Parameters at 100 K

bond	distance, Å	bond angle	angle, deg
C(1)−C(2)	1.5317(1)	C(2)−C(1)−C(2′	112.46(1)
C(2)−O(3)	1.4463(2)	C(2′−C(1)−C(2″	107.998(5)
C(2)−H(2A)	1.092	C(1)−C(2)−H(2A)	110.22(1)
C(2)−H(2B)	1.092	C(1)−C(2)−H(2B)	110.450(9)
O(3)−N(1)	1.4009(2)	H(2A)-C(2)−H(2B)	108.65(1)
N(1)−O(1)	1.1994(2)	C(1)−C(2)−O(3)	106.774(8)
N(1)−O(2)	1.2057(2)	C(2)−O(3)−N(1)	112.95(1)
		O(3)−N(1)−O(1)	118.01(1)
		O(3)−N(1)−O(2)	112.46(1)
		O(1)−N(1)−O(2)	129.53(2)

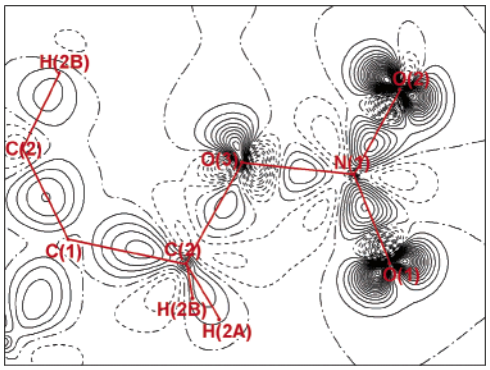

(a)

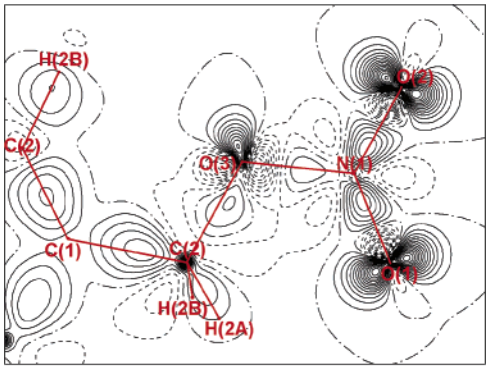

(b)

Figure 3. Experimental (a) and theoretical (b) static deformation electron density maps in the C(2)−O(1)−O(2) plane. Contour interval is 0.1 eÅ^{-3}. Positive contours are solid, negative are dashed, and the zero line is dash−dotted.

Results and Discussion

The PETN molecule has $\bar{4}$ point symmetry, and selected geometrical parameters at 100 K are listed in Table 2. All the bond distances and angles agree reasonably well with the values reported previously.[13,20,21] The C(1), C(2), and O(3) atoms have slightly distorted tetrahedral geometries, whereas the nitrogen atom is close to an sp^2 hybridization state, with the O(1)−N(1)−O(2) angle being higher than 120°, in agreement with the VESPR theory (Table 2, Figure 1). The C(2)−O(3)−N(1)−O(1)−O(2) fragment remains practically flat with a maximum deviation from the mean plane of 0.027 Å for the O(3) atom. Static (model) deformation electron density maps are shown in Figure 3 and the Laplacian of the total electron density maps are presented in Figures 4 and 5. Each expected covalent bond manifests itself as a significant deformation−electron density peak; corresponding areas of electron concentration are also seen from the Laplacian maps. For each oxygen atom, two electron

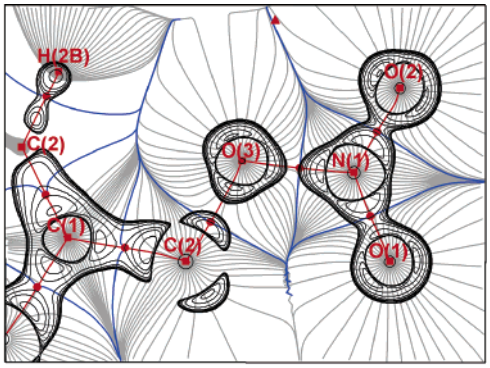

(a)

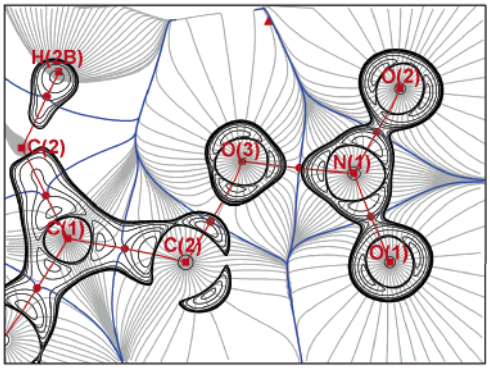

(b)

Figure 4. Negative part of the Laplacian of the experimental (a) and theoretical (b) electron density in the C(2)−O(1)−O(2) plane, overlaid with gradient lines in the electron density. (3,−3) critical points (maxima) are shown as red squares, (3,−1) bond critical points are red circles, (3,+1) ring critical point is shown as red triangle; gradient lines are gray, bond paths are red and projections of the atomic zero-flux surfaces are shown as blue lines. The Laplacian isocontours are −(1.2, 2, 4, 8, 12, 20, 40, 80, 120, 200, 400) eÅ^{-5}.

density concentrations associated with electron lone pairs (LP) have been found. For the NO_2 oxygen atoms, the LP's are located in the $-NO_3$ plane almost perpendicular to the N−O bonds with the N(1)−O(1)−LP(1,2) angles being 94.4 and 98.3°, and the N(1)−O(2)−LP′(1,2) angles[33] being 101.4 and 97.0°. A very similar picture has been observed for the NO_2 groups in the explosives[34] NTO,[4] biguanidinium, and ammonium dinitramides,[5,7] TNDAP,[9] as well as in the nonexplosives 1-phenyl-4-nitroimidazole,[35] *p*-nitroaniline,[36] and N_2O_4.[37] For the central O(3) atom, a close to tetrahedral arrangement of its bonds and lone pairs might be anticipated, but the two LP's (Figure 5) form an angle LP(1)−O(3)−LP(2) of ∼140° for the theoretical results, with the N(1)−O(3)−LP(1) and N(1)−O(3)−LP(2) angles[33] being 97 and 101°, respectively. For the experimental data, the LP(1)−O(3)−LP(2) angle is even bigger (171°) with the N(1)−O(3)−LP(1) and N(1)−O(3)−LP(2)

(33) Based on the position of the (3,+3) critical points in the Laplacian, theoretical case.
(34) Abbreviations for the explosive materials are as follows: 5-nitro-2,4-dihydro-3H-1,2,4-triazol-3-one [NTO]; biguanidinium dinitramide [(BIGH)-(DN)]; biguanidinium bis-dinitramide [$(BIGH_2)(DN)_2$]; 1,3,4-trinitro-7,8-diazapentalene [TNDAP]; ammonium dinitramide [ADN]; 2,4,6,8,10,12-hexanitrohexaaza-isowurtzitane [HNIW or CL-20]; Pentaerythritol tetranitrate [PETN].
(35) Kubicki, M.; Borowiak, T.; Ditkiewicz, G.; Souhassou, M.; Jelsch, C.; Lecomte, C. *J. Phys. Chem. B* **2002**, *106*, 3706−3714.
(36) Volkov, A.; Abramov, Yu.; Coppens, P.; Gatti, C. *Acta Crystallogr.* **2000**, *A56*, 332−339.
(37) Messerschmidt, M.; Wagner, A.; Wong, M. W.; Luger, P. *J. Am. Chem. Soc.* **2002**, *124*, 732−733.

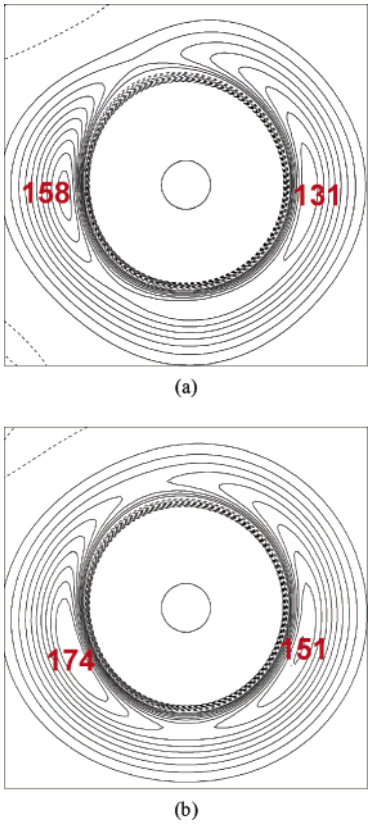

Figure 5. The Laplacian of the experimental (a) and theoretical (b) electron density around the O(3) atom in the plane of its lone pairs. Numbers indicate $-\nabla^2\rho(\mathbf{r})$ values at the (3,+3) CPs in the Laplacian. Contour interval is 15 eÅ^{-5}.

angles being 94 and 92°, respectively. No hydrogen bonds with the O(3) atom have been found in the crystal (see below).

Table 3 lists all the intramolecular (3,−1) bond critical points; their positions along with the associated bond paths are shown in Figure 4. Generally, good agreement between theory and experiment is observed for the electron density values. For the Laplacian values, the agreement is less satisfying, mostly due to the difference in the λ_3 values related to the deficiency of the multipole model description of the electron density.[36,38] The bonds C(1)−C(2), C(2)−O(3), and C(2)−H(A,B) can be considered as single bonds, whereas all three N−O bonds are conjugated, as expected, with the highest ellipticity being for the N(1)−O(3) bond. However, as noted in previous studies of nitro compounds, the ellipticities of N−O bonds are much less than for C═C or C═O bonds.

Topological bond orders[38,39] have been calculated from the electron density values (ρ) and the principle electron-density curvatures (λ_1, λ_2, λ_3) at the bond critical points (Table 3) as $n_{\text{topo}} = a + b\lambda_3 + c(\lambda_1 + \lambda_2) + d\rho_{\text{CP}}$, all values in atomic units. The following coefficients were used: for the C−C bond[39] $a = -0.522$, $b = -1.695$, $c = 0$, $d = 8.473$; for the C−O bond[38] $a = -0.427$, $b = 0.280$, $c = -0.240$, $d = 6.464$; for the C−H bonds[40] $a = 0.128$, $b = 0.246$, $c = 0.480$, $d = 4.926$. For the N−O bond, we have obtained the following coefficients: $a = -0.628$, $b = 0.505$, $c = 0.448$, and $d = 5.275$ (the correlation coefficient $R = 0.97$ and the rms deviation 0.02). These parameters were obtained from molecular theoretical calculations by the fit of the above-mentioned expression for n_{topo} to the Cioslowski & Mixon[41] bond orders; the procedure described by Howard & Lamarche[39] and Tsirelson et al.[38] has been used. In general, the bond orders for a total of 63 N−O bonds were used in the calculations, including the −O−N−O bond in PETN. Table 3 shows that, according to the bond-order values, the C−C, C−O, and C−H bonds in PETN are single, as expected, with an average bond order value of 0.91. The N−O(1,2) bond order is 1.94 on average, and the N−O(3) bond order is 1.16, both values reflecting the conjugation of the electron density in the $-NO_3$ fragment.

Contrary to the assumption in the literature (see, for example, ref 42) that the O−NO_2 bond is the weakest in the molecule, our study[43] of the bond CP properties shows that this bond is relatively strong. Indeed, it is characterized by high electron-density value ($\rho_b = 2.2$ eÅ^{-3}), moderately high ellipticity (0.17), and a bond order which exceeds unity (1.16). At the same time, the Laplacian value is the lowest for this bond. This bond is, probably, stronger than the C(1)−C(2) and C(2)−O(3) bonds (with ρ_b of about 1.6 eÅ^{-3}), which are shown to be first to break when the crystal is exposed to a high energy laser, high energy fracture or high pressure.[10,42,44] In contrast, it has been demonstrated that the O−NO_2 bond breaks as the initial step in cases of slow thermal decomposition or exposure to low energy fracture or low energy laser at ambient pressure[42,45] with a dissociation energy of 164.2 kJ/mol.[46]

Three relatively weak hydrogen bonds have been found in the PETN crystal (Figure 2); the properties of the corresponding bond critical points are listed in Table 4. The interatomic distances for these hydrogen bonds vary between 2.3 and 2.7 Å, and the dissociation energies vary between 4.2 and 6.4 kJ/mol as determined from the potential energy density at the critical point.[47] Weaker oxygen−oxygen bonding interactions[6] have been found in the PETN crystal as well. For every O···H and O···O interaction from the experimental data, a bond path (Figure 6) and the associated virial path have been found, which demonstrate the bonding character of these interactions.[48] We have to note, however, that the bond path joining the O(2)··· O(3(1/2 − y, 1/2 − x, 1/2 + z)) atoms in the experimental case, points toward the nitrogen atom in the theoretical case (Table 4), and no virial path has been found for this possible O(2)··· N(1) interaction.

Topological atomic valence indexes (Table 5), calculated according to Tsirelson et al.[38] as a sum of the bond-order values over each atom (V_{topo}), show that the most reactive atoms in the molecule are oxygens and hydrogens. These are the atoms participating in numerous interatomic bonding interactions, with

(38) Tsirelson, V. G.; Stash, A. I.; Potemkin, V. A.; Rykounov, A. A.; Shutalev, A. D.; Zhurova, E. A.; Zhurov, V. V.; Pinkerton, A. A.; Gurskaya, G. V.; Zavodnik, V. E. *Acta Crystallogr.* **2006**, *B62*, 676−688.
(39) Howard, S. T.; Lamarche, O. *J. Phys. Org. Chem.* **2003**, *16*, 133−141.
(40) Bartashevich, E. V.; Potemkin, V. A.; Stash, A. I.; Tsirelson, V. G. *Proc. IV National Crystal Chemistry Conference June 26−30 2006*, Chernogolovka, Russia; p 5.7.
(41) Cioslowski J.; Mixon S. T. *J. Am. Chem. Soc.* **1991**, *113*, 4142−4145.
(42) Ng, W. L.; Field, J. E.; Hauser, H. M. *J. Appl. Phys.* **1986**, *59*, 3945−3952.
(43) We assume that the "strength" of the bond is directly proportional to the electron density value at the bond critical point; the approximate values of the total electronic energy, calculated using the kinetic energy expansion (Kirzhnits, D. A. *Sov. Phys. JETP* **1957**, *5*, 64−71) and the virial theorem (ref 14) demonstrate the same tendency.
(44) Naud, D. L.; Brower, K. R. *J. Org. Chem.* **1992**, *57*, 3303−3308.
(45) Hiskey, M. A.; Brower, K. R.; Oxley, J. C. *J. Phys. Chem.*. **1991**, *95*, 3955−3960.
(46) Khrapovskii, G. M.; Shamsutdinov, T. F.; Chachkov, D. V.; Shamov, A. G. *J. Mol. Struct. (THEOCHEM)* **2004**, *686*, 185−192.
(47) Espinosa, E.; Molins, E. *J. Chem. Phys.* **2000**, *11*, 5686−5694.
(48) Bader, R. F. W. *J. Phys. Chem. A* **1998**, *102*, 7314−7323.

Table 3. Bond Critical Points in the PETN Crystal: Intramolecular Bonds[a]

bond	ρ, eÅ^{-3}	$\nabla^2\rho$, eÅ^{-5}	R_{ij}, Å	d_1, Å	d_2, Å	λ_1, eÅ^{-5}	λ_2, eÅ^{-5}	λ_3, eÅ^{-5}	e	n_{topo}
C(1)−C(2)	1.640	−11.11	1.532	0.738	0.797	−11.683	−9.799	10.373	0.19	0.806
	1.655	−11.21		0.737	0.798	−11.477	−10.611	10.878	0.08	0.788
C(2)−O(3)	1.628	−12.24	1.446	0.584	0.865	−12.944	−11.224	11.927	0.15	0.907
	1.610	−9.06		0.596	0.853	−12.010	−10.786	13.736	0.11	0.928
C(2)−H(2A)	1.923	−20.58	1.092	0.713	0.379	−18.941	−17.983	16.347	0.05	0.963
	1.916	−19.58		0.735	0.357	−19.123	−18.408	17.951	0.04	0.962
C(2)−H(2B)	1.938	−20.17	1.092	0.728	0.364	−19.649	−18.191	17.671	0.08	0.969
	1.880	−17.79		0.739	0.353	−18.752	−17.682	18.644	0.06	0.964
O(3)−N(1)	2.234	−1.75	1.401	0.725	0.678	−20.212	−17.175	35.637	0.18	1.171
	2.121	1.47		0.721	0.682	−18.927	−16.167	36.560	0.17	1.145
O(1)−N(1)	3.675	−22.26	1.199	0.617	0.585	−34.787	−30.841	43.372	0.13	1.935
	3.464	−13.97		0.617	0.585	−31.528	−30.030	47.590	0.05	1.933
O(2)−N(1)	3.570	−16.57	1.206	0.619	0.588	−32.103	−29.186	44.722	0.10	1.962
	3.430	−12.60		0.616	0.591	−30.790	−29.392	47.580	0.05	1.934

[a] First line − experiment, second line − theoretical calculation; ρ is the electron density; $\nabla^2\rho$ is the Laplacian; R_{ij} is interatomic distance; d_1 and d_2 are the distances from the critical point to atoms 1 and 2, respectively; λ_1, λ_2, λ_3 are principle curvatures; ϵ is bond ellipticity; n_{topo} is topological bond order. Average standard deviations are 0.02 eÅ^{-3} for the electron density and 0.08 eÅ^{-5} for the Laplacian.

Table 4. Bond Critical Points in the PETN Crystal: Intermolecular Interactions[a]

bond[b]	ρ, eÅ^{-3}	$\nabla^2\rho$, eÅ^{-5}	R_{ij}, Å	d_1, Å	d_2, Å	λ_1, eÅ^{-5}	λ_2, eÅ^{-5}	λ_3, eÅ^{-5}	g, au	v, au	h_e, au	D_e, kJ/mol
O(1)···H(2A)$^{(1)}$	0.060	0.79	2.318	1.403	0.970	−0.299	−0.271	1.362	0.00657	−0.00492	0.00165	6.46
	0.062	0.96	2.318	1.390	0.938	−0.285	−0.248	1.494	0.00792	−0.00573	0.00219	7.52
O(2)···H(2B)$^{(2)}$	0.039	0.87	2.439	1.470	0.972	−0.150	−0.113	1.136	0.00657	−0.00409	0.00248	5.37
	0.048	0.85	2.439	1.446	1.006	−0.199	−0.155	1.201	0.00666	−0.00449	0.00217	5.89
O(2)···H(2B)$^{(3)}$	0.038	0.63	2.708	1.506	1.259	−0.120	−0.066	0.811	0.00485	−0.00320	0.00164	4.20
	0.037	0.64	2.708	1.504	1.238	−0.111	−0.090	0.838	0.00496	−0.00323	0.00173	4.24
O(2)···O(3)$^{(4)}$	0.041	0.70	3.030	1.485	1.553	−0.143	−0.071	0.910	0.00540	−0.00358	0.00182	4.70
O(2)···N(1)$^{(4)}$	0.041	0.65	3.043	1.491	1.565	−0.134	−0.023	0.805	0.00507	−0.00341	0.00166	4.48
O(1)···O(1)$^{(5)}$	0.025	0.51	3.147	1.573	1.573	−0.070	−0.050	0.632	0.00379	−0.00228	0.00151	2.99
	0.028	0.52	3.147	1.574	1.574	−0.076	−0.057	0.653	0.00397	−0.00246	0.00151	3.23
O(1)···O(2)$^{(5)}$	0.024	0.43	3.228	1.595	1.637	−0.065	−0.041	0.536	0.00321	−0.00197	0.00124	2.59
	0.024	0.43	3.228	1.602	1.636	−0.062	−0.031	0.524	0.00326	−0.00198	0.00127	2.60
O(1)···O(2)$^{(6)}$	0.018	0.32	3.312	1.650	1.661	−0.048	−0.045	0.411	0.00235	−0.00139	0.00096	1.82
	0.017	0.32	3.312	1.650	1.663	−0.047	−0.040	0.407	0.00237	−0.00140	0.00097	1.84
O(1)···O(2)$^{(7)}$	0.017	0.32	3.323	1.669	1.657	−0.057	−0.038	0.415	0.00234	−0.00137	0.00097	1.80
	0.018	0.32	3.323	1.675	1.656	−0.044	−0.028	0.395	0.00243	−0.00145	0.00098	1.90
O(1)···O(3)$^{(8)}$	0.013	0.24	3.426	1.709	1.720	−0.043	−0.031	0.314	0.00175	−0.00100	0.00074	1.31
	0.013	0.24	3.426	1.708	1.718	−0.035	−0.029	0.304	0.00177	−0.00102	0.00076	1.34

[a] First line − experiment, second line -theoretical calculation; ρ is the electron density; $\nabla^2\rho$ is the Laplacian; R_{ij} is interatomic distance; d_1 and d_2 are the distances from the critical point to atoms 1 and 2, respectively; λ_1, λ_2, λ_3 are principle curvatures; g, v and h_e are the kinetic, potential, and total electronic energies at the critical point, respectively. D_e is the dissociation energy calculated as $D_e = -v/2$ (ref 47). [b] Symmetry operators: (1) $(1/2 + y - 1, 1/2 + x, 1/2 + z)$; (2) $(y, -x, -z + 1)$; (3) $(1/2 + x, 1/2 - y, 1/2 - z)$; (4) $(1/2 - y, 1/2 - x, 1/2 + z)$; (5) $(-x, -y + 1, z)$; (6) $(1/2 + y - 1, 1/2 + x, 1/2 + z - 1)$; (7) $(-y, x, -z + 1)$; (8) $(1/2 + x - 1, 1/2 - y, 1/2 - z)$.

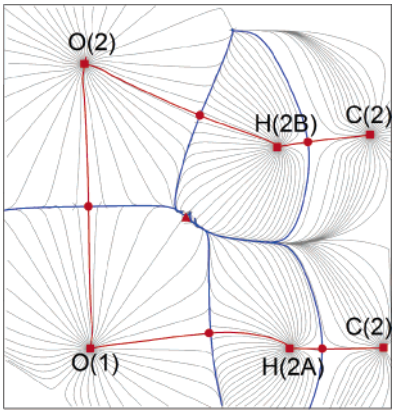

Figure 6. The oxygen−hydrogen and oxygen−oxygen bonding interactions: gradient paths in the experimental electron density in the O(1)···H(2A)···O(2) plane. For definitions, see Figure 4.

the O(1) and O(2) atoms having slightly lower V_{topo} values and participating in a larger number of interactions than the O(3) atom (Table 4). This crystal packing is very different from the prototype Pentaerythritol crystal (PE), where molecules are packed in layers perpendicular the crystallographic *c*-axis.[49,50]

All the explosive materials studied with the QTAIM analysis so far[4−9,51,52] are particularly rich in closed-shell intra- and interatomic interactions; they are significantly multiplied in number by the high symmetry in the PETN crystal (corresponding figures have been deposited). Although not all of our results have been completely published, O···O, O···N, O···C, O···H, N···N, and N···H interactions have been found in NTO crystals; O···O, O···N, O···C, and O···H in TNDAP; O···O, O···N, and O···H in ADN; O···O, O···N, O···H, N···N, and N···H in (BIGH)(DN) and $(BIGH_2)(DN)_2$; O···H, O···O, and O···N in γ−CL20 and ϵ−CL20.[34] Klapötke et al.[51] reported O···O and O···N interactions in the 1,5-diamino-4-methyl-tetrazolium dinitramide crystal. It has been proposed[53] that prior to an explosion, rupture of these weak interactions, for example, by

(49) Zhurov, V. V.; Zhurova, E. A.; Chen, Y.-S.; Pinkerton, A. A. *J. Appl. Crystallogr.* **2005**, *38*, 827−829.
(50) Zhurova, E. A.; Tsirelson, V. G.; Zhurov, V. V.; Stash, A. I.; Pinkerton, A. A. *Acta Crystallogr.* **2006**, *B62*, 513−520.
(51) Klapötke, T. M.; Mayer, P.; Schulz, A.; Weigand, J. J. *J. Am. Chem. Soc.* **2005**, *127*, 2032−2033.
(52) Pinkerton, A. A.; Zhurova, E. A.; Chen, Y.-S. In *Energetic Materials. Theoretical and Computational Chemistry Series*; Politzer, P., Murray, J. S., Eds.; Elsevier: New York, 2003; Vol. 12, pp 215−245.
(53) Bader, R. F. W. Personal communication, 2006.

Table 5. Atomic Charges (q), Volumes (Ω), Total Electronic Energies (H_e) Integrated over Atomic Basins and Atomic Topological Valence Indexes (V_{topo})[a]

atom	q, e^-	$q^{procrystal}$, e^-	δq, e^-	Ω, Å^3	$\Omega^{procrystal}$, Å^3	$\delta\Omega$, Å^3	$-H_e$, au	V_{topo}
C(1)	0.118	0.008	0.110	5.96	6.30	−0.34	38.253	3.224
	0.158	0.008	0.150	5.80	6.30	−0.50	38.255	3.152
C(2)	0.272	0.033	0.239	7.24	8.71	−1.47	38.237	3.645
	0.172	0.033	0.139	7.30	8.71	−1.41	38.451	3.642
O(1)	−0.400	−0.204	−0.196	16.22	14.75	1.47	75.238	1.931
	−0.365	−0.204	−0.161	16.08	14.75	1.33	75.175	1.924
O(2)	−0.417	−0.191	−0.226	16.27	14.55	1.72	75.188	1.938
	−0.371	−0.191	−0.180	15.94	14.55	1.39	75.195	1.917
O(3)	−0.688	−0.347	−0.341	13.44	12.19	1.25	75.480	2.064
	−0.542	−0.347	−0.195	13.24	12.19	1.05	75.312	2.056
N(1)	0.906	0.414	0.492	6.36	7.71	−1.35	53.959	5.026
	0.769	0.414	0.355	6.72	7.71	−0.99	54.111	4.969
H(2A)	0.143	0.151	−0.008	4.81	5.52	−0.71	0.589	0.963
	0.161	0.151	0.010	4.86	5.52	−0.66	0.558	0.962
H(2B)	0.157	0.145	0.012	5.20	6.08	−0.88	0.571	0.969
	0.137	0.145	−0.008	5.44	6.08	−0.64	0.564	0.964
Molecule	0.002	0.016	−0.014	284.11	284.36	−0.25	1315.301	
	0.006	0.016	−0.010	284.19	284.36	−0.17	1315.719	

[a] First line − experiment, second line − theoretical calculation; $\Omega_{unit\ cell}/2 = 283.26$ Å^3; $H_e^{Crystal98}/2 = -1316.250$ au; $L_{err}^{molecule} = 0.00005$ au (experiment), 0.00007 au (theory), 0.00012 au (procrystal), $L_{err} = (\Sigma L_\Omega^2/N_{atoms})^{1/2}$, L_Ω is the atomic integrated Lagrangian.[56]

Table 6. NO_2 Group Atomic Integrated Properties: Charges (q), Volumes (Ω), Total Electronic Energies (H_e), and Electronic Energy Per Mole (H_e/M)

	q, e^-		Ω, Å^3		$-H_e$, au		$-H_e$/M
	O	N	O	N	O	N	molecule
nonexplosives:							
p-nitroaniline,[57] average values	−0.45	0.18	17.2	7.9			
1-phenyl-4-nitroimidazole[35]	−0.35, −0.48	0.21	17.6, 17.0	8.2			
N_2O_4[37]	−0.24	0.46	15.5	7.9			
explosives:							
NTO[4,8]	−0.35, −0.38	0.50	15.2, 16.3	6.7	75.03, 75.05	54.32	4.014
(BIGH)(DN) [5,8]	−0.47, −0.60	0.65	14.7, 15.7	6.1	75.13, 75.36	54.05	3.935
	−0.42, −0.34	0.71	14.5, 17.2	6.3	74.84, 74.58	53.87	
$(BIGH_2)(DN)_2$ [5,8]	−0.58, −0.53	0.64	15.2, 14.4	6.3	75.63, 75.45	54.26	4.088
	−0.54, −0.59	0.60	15.4, 14.6	6.4	75.47, 75.62	54.31	
1,5-diamino-4-methyl-tetrazolium dinitramide [51]	−0.50, −0.50	0.63					
	−0.55, −0.56	0.64					
TNDAP[9]	−0.47, −0.46	0.43	15.9, 16.5	7.0	74.76, 74.69	54.00	3.947
	−0.51, −0.55	0.35	16.1, 16.9	7.6	74.85, 75.02	54.26	
	−0.48, −0.40	0.40	15.6,17.9	8.5	74.77, 74.55	54.15	
ADN [7]	−0.46, −0.54	0.60	15.5, 15.1	6.6	75.14, 75.39	54.16	4.200
	−0.54, −0.54	0.66	14.8, 14.0	6.0	75.17, 75.49	54.19	
PETN (this work)	−0.40, −0.42	0.91	16.2, 16.3	6.4	75.24, 75.19	53.96	4.160

lattice deformation under impact, would sufficiently destabilize the crystal to initiate the explosive reaction. Further studies will reveal the importance of these interactions for explosive materials.

Table 5 lists the atomic volumes, charges, and total electronic energies integrated over the atomic basins delimited by the zero-flux surfaces[14] for the experimental data and the solid state calculation. The integrated Lagrangian for every atom was reasonably small, demonstrating the accuracy of the integrations. All the atomic charges sum to very small values, thus confirming that the molecule is practically electroneutral as required. The sums of the atomic volumes reproduce the unit cell volume per molecule with an error of 0.3%. We have also calculated the atomic charges and volumes for the PETN procrystal again using zero-flux surface partitioning.[54] For all atoms, except carbons, the procrystal "atomic charges" are significantly different from zero. The "deformation charges",[8] $\delta q = q_{AIM} - q_{AIM}^{pro}$, are smaller in value than the charges described above, and they reflect the interatomic electron transfer which accompanies the molecule and crystal formation. In the same way, the differences in atomic volumes, $\delta\Omega$, reflect how the atomic volumes change upon formation of the molecule or crystal from neutral atoms. The oxygen atoms become much more negative, and their atomic volumes are increased, as anticipated. The carbon and nitrogen atoms become more positive, and their atomic volumes become smaller; whereas for the hydrogen atoms the deformation charges are close to zero, but their volumes significantly decrease during crystal formation. The sums of the total electronic energies integrated over the atomic basins[8,55] agree well with the total energies calculated with wave functions using *CRYSTAL98* (within 0.07%). It is of interest to compare these integrated properties for the explosive PETN with other compounds available in the literature, especially for the "energetic" NO_2 group. The currently available data are listed in Table 6. Comparing the explosive with nonexplosive materials, there is an apparent enhancement of nitrogen charge and

(54) Maslen, E. N.; Spackman, M. A. *Aust. J. Phys.* **1985**, *38*, 273−287.

(55) Tsirelson, V. G.; Stash, A. I. *Acta Crystallogr.* **2004**, *A60*, 418−426.
(56) Flensburg, C.; Madsen, D. *Acta Crystallogr.* **2000**, *A56*, 24−28.
(57) Volkov, A.; Gatti, C.; Abramov, Yu.; Coppens, P. *Acta Crystallogr.* **2000**, *A56*, 252−258.

reduction in all atomic volumes. As the integrated energies are not available for the four additional compounds found in the literature, only the atomic energies for the six explosives can be compared. These explosives cover a significant range of shock sensitivities, with ADN and PETN being the most sensitive in this list.[11] We observe that the molecular electronic energy per mole is the largest for these two crystals, but the available sample of compounds is still too small to draw unambiguous conclusions.

Conclusion

In this work, the microscopic properties of explosive materials obtained from X-ray diffraction experiments has been extended to include topological bond orders and topological atomic valence indexes, as well as analysis of all intermolecular bonding interactions. A possible relationship between intermolecular interaction energies and shock sensitivity has been proposed.

Acknowledgment. We thank Prof. Richard Bader for valuable discussions. This work was supported by the Office of Naval Research through the contract number N00014-05-1-0397, the Russian Federal Agency for Education (Program "Development of the Highest-School Scientific Potential, 2006-2008", Project 2.1.1. 5051), and the Russian Foundation for Basic Research (Grant 04-03-33053).

Supporting Information Available: Crystallographic CIF-file and packing diagrams showing all intermolecular interactions in the crystal. This material is available free of charge via the Internet at http://pubs.acs.org.

JA0658620